Evaluation of Circular Aperture Transmission Coefficients in the Presence Of Obscurations

J. G. Davis, P. Shakespeare, and N. Kiley

BAE Systems, Military Air Solutions, Electromagnetic Engineering, W423
Warton Aerodrome, Preston, PR4 1AX, United Kingdom
john.g.davis@baesystems.com

Abstract ─ This paper describes a novel parametric approach to the simulation of circular aperture transfer functions in the presence of obscurations at microwave frequencies. A novel virtual 'absorbing box' power loss integration technique is applied to successfully demonstrate its validity for conditions where the aperture diameter approaches one tenth of the plate largest dimension.

Index Terms ─ Aperture, diffraction, transmission coefficient.

I. INTRODUCTION

The formulation of the transmission coefficient for a circular aperture in a plate of finite cross section has been the subject of much scientific interest over the years [1, 2]. The complex nature of the complete solution has lead to a variety of approximate empirical formulations based on uni-mode propagation models. Amongst these is the simple Huygens wavefront approach adopted by Koch/Airy which produces an impressive correlation with experimental data [1]. However, this method breaks down for larger apertures where multi-mode propagation prevails. Hybrid solutions attributable to Seshadri & Wu [3], based on a truncated form of the infinite modal series, have been formulated to accommodate larger apertures. Historically, these are preferred to rigorous solutions incorporating all propagating and evanescent modes as these require the implementation of intricate mode matching techniques [4]. In this paper, a novel, alternative parametric solution based on the Seshadri formulation is proposed. This yields an elementary basis function which can be readily applied to bounded apertures both in isolation and in cavity based mode stirred reverberation conditions. The development of the parametric algorithm is described first followed by comparisons with a transmission line method (TLM) solver simulation, which employs a novel means of eliminating diffraction at the aperture plate edges. The method is further expanded to incorporate diffraction shadow attenuation effects and multiple reflection modulation arising from obscurations.

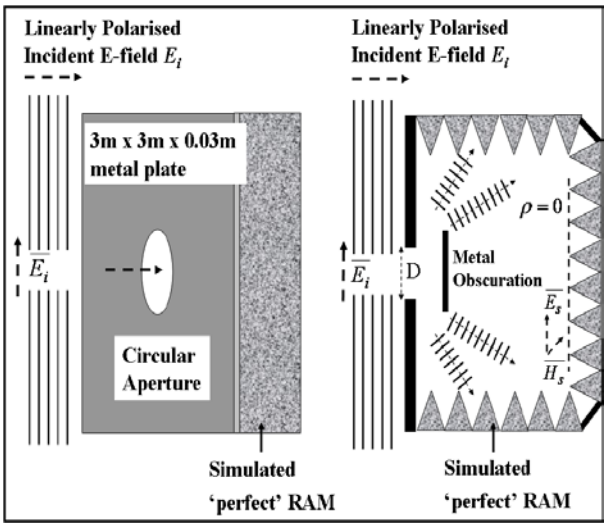

Fig. 1. TLM numerical circular aperture model showing the virtual absorbing box used for edge diffraction elimination.

II. APERTURE FINITE DIFFERENCE SIMULATIONS

The first step in producing the aperture transmission numerical solution: comprise a reduction in the considerable 9 m^3 modelled mesh volume in order to minimise simulation run times.

Submitted On: May 23, 2011
Accepted On: October 20, 2011

As the aperture is a symmetrical shape with two planes of symmetry, it is possible to define orthogonal electric and magnetic wall boundary conditions in order to reduce the computational domain by a factor of 3 quarters. Secondly, as the aperture plate dimensions are limited within the modelling constraints of the chosen transmission line method (TLM) solver, there may be an undesirable leakage of energy around the plate periphery due to edge diffraction. Suppression of this phenomena, however, may be effected via the introduction of a virtual 'absorbing box' coincident with the plate edges and boundary mesh perfect matched layer shown in Fig. 1. If the box walls are configured within the TLM solver as metallic sheets with a $377\,\Omega$ surface impedance (i.e equal to the characteristic impedance of unbounded propagating waves with the box volume), then the reflection coefficient at the interior box walls will be zero. Under these circumstances all energy impinging on the interior will be absorbed at the walls. Conversely, the exterior boundaries of the box present a surface impedance of zero to any external waves diffracted around its periphery, thus resulting in total external reflection. Under these conditions, the interior walls behave as a perfect matched layer (PML) and the exterior walls as perfect reflecting surfaces. The computation of the aperture transmitted power may then be effected via the selection of the CST microstripes, the TLM solver 'integrate loss over volume' and 'integrate loss over surface' output options, thus enabling computation of the aperture transmission coefficient from the ratio of energy transmitted to that absorbed in the RAM enclosure. This absorbing mechanism is analogous to that of radar absorbent material (RAM) found in an anechoic chamber as illustrated symbolically in Fig. 1.

A. Absorbing box simulation

Essentially, the aperture transmission coefficient is simulated via exploitation of the CST microstripes, in-built wall loss calculation capability [5]. The configuration of Fig. 1 used for this purpose, comprises a perfect RAM absorbing box modelled as a basic 'enclosure' shape with 3 mm thick walls. The enclosure aperture face is formed from a 3 mm thick copper plate with 400 mm diameter circular aperture located at its centre. The materials chosen to configure the RAM enclosure and aperture respectively, i.e copper plate of conductivity 5.8 x 10^7 S/m and absorbing box of $377\,\Omega$ surface impedance, ensured total containment and absorption of transmitted energy by the enclosure walls. The plane wave signal excitation, derived from a gaussian pulse source positioned 0.5 m in front of the aperture, was monitored in *E* and *H-field* cartesian component form at various points along the absorbing enclosure axis. The cuboidal PML simulation boundary, comprising dimensions 10% greater than the complete absorbing enclosure, was discretised to provide sufficient plate and aperture edge resolution without incurring excessive run times. A summary of all modelling parameters including system bandwidth, run and time step duration are detailed in Table 1 above.

Table 1: Aperture model simulation parameters

CST Simulation Parameter	Value
Simulation Bandwidth	0.01 to 3 GHz
Run Duration	10 μs
No. of timesteps	6153
Total run time	30 mins
Number of cells	212,589
Maximum Cell Size	9.88 mm
Metal Plate Dimensions	3.x 3.x 0.003 m
Absorbing Enc. Dimensions	3.x 3. x 0.5 m
Conductivity (Metal Plate)	$5.8\text{x}10^{-7}$ S/m
Encl. Surface Impedance	377 Ω

III. TRANSMISSION COEFFICIENT MODELLING

The TLM solver, simulated transmission coefficient, is defined as the ratio of the total power transmitted through the aperture (i.e that dissipated on the inside of the absorbing box) to that power incident on the aperture of diameter D, as derived from the Poynting theorem, i.e :

$$S = \frac{\frac{1}{2}\mathrm{Re}\iint_{\cdot}\left(\overline{E_s}\times\overline{H_s}^{*}\right)dA}{\pi D^2\left|E_i\right|^2/\eta_0}, \qquad (1)$$

where $\mathbf{E_s}$ and $\mathbf{H_s}$ are the electric and magnetic vector fields on the inside surface of the 'perfect RAM' absorbing box in Fig. 1 and $\mathbf{E_i}$ is the incident *E-field* at the aperture. The transmission coefficients S, attributable to the theoretical formulations of Seshadri [3] and Andrewski [6],

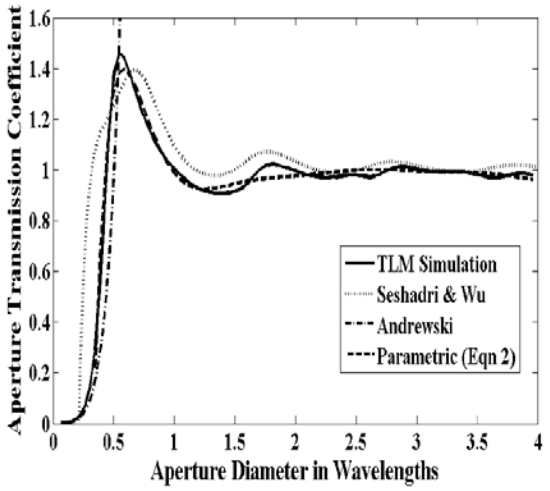

Fig. 2. Comparison of simulated transmission coefficients showing theoretical, simulated, and parametric solutions.

are plotted along with the equivalent TLM simulation as a function of the aperture diameter in wavelengths in Fig. 2. A comparison of the resulting profiles reveals a strong correlation between theoretical and modelled responses at the start of the wave number (kD) range for the Andrewski formulation (i.e 0<kD<1/pi), and in the latter part of the range for the Seshadri case (3/pi<kD<10/pi). These features enable a hybrid solution (2) to be formulated combining the functional dependencies attributable to both [3] and [6], thereby yielding an equivalent parametric response for the composite range as :

$$A_p(\omega) = \frac{\begin{array}{l}1 - \gamma^{-3/2}a_1(\sin\varphi) + \gamma^{-2}(a_2 + a_3\sin 2\varphi) - \ldots \\ \ldots. a_6(a_4 + a_5\sin 2\varphi)\gamma^{-5/2}\end{array}}{a_7 K \exp -[a_8(a_9 + K)]/\pi}, \quad (2)$$

where $\gamma = D/\lambda$, $\varphi = 2\gamma - \pi/4$. The coefficients a_n in the parametric function, optimised to provide the 'best fit' using the inversion algorithm specified in [10], are defined as:

$$a = \begin{bmatrix} -0.163 & -0.950 & 0.039 & -1.042 \ldots \\ -0.058 & 0.490 & -0.744 & 0.601 & -1.118 \end{bmatrix}. \quad (3)$$

A comparison between the optimised parametric and TLM simulated responses in Fig. 2 yields an impressive correlation, demonstrating the validity of the function of (2) as an elementary, universal transmission coefficient representation applicable to circular apertures of any dimension.

IV. APERTURE OBSCURATION MODELLING

The modelling of aperture transmission coefficients in the presence of blockages or obscurations is an important element in the analysis of the energy transfer between cavities and equipment bays in aircraft and ships, as the geometry of adjoining bay openings and physical obstructions within its proximity, ultimately determines the extent of the internal energy transfer within the structure [7, 8]. In this section, a method of modelling the perturbing effect of a metal plate, positioned in close proximity to a circular aperture, is established for any given aperture diameter in wavelengths.

A. Obscuration theory

The modulation of the open aperture transmission coefficient for a square obscuration plate twice the width of the aperture shown in Fig. 1, may be modelled as the convolution of three distinct functions, i.e the open aperture transfer algorithm of (2), a blockage or obscuration function, and a multiple reflection standing wave function. The obscuration function, may be derived via application of the standard geometric diffraction theory to the resultant scattered signal at the plate edges. This analysis requires the evaluation of the Fresnel-Kirchoff diffraction parameter [9] at the obscuration plate boundaries. Application of this theory to the upper and lower knife edges in Fig. 3 yields :

$$v_u(\omega) = \alpha_u\left[\frac{\omega L d}{\pi c_0(L+d)}\right];\ v_l(\omega) = \alpha_l\left[\frac{\omega L d}{\pi c_0(L+d)}\right], \quad (4)$$

where the orthogonal symmetry of the box and aperture, enables an identical result to be derived for the plate left and right, vertical edges. The complex Fresnel integrals, representing the sum of all secondary Huygens sources on each of the upper and lower plate edges may be expressed in terms of their diffraction parameters v_u as :

$$F_u(\omega) = \int_0^{v_u(\omega)} \exp\left(-j\pi v^2\right) dv, \quad (5)$$

and similarly for v_l. The resultant scattered field in the shadow region beyond the plate in Fig. 3, attributable to a given edge, may be derived via integration of the Fresnel parameters v in (5) as :

$$E = 0.5(1 + j)(0.5(1 - j) - F(\omega)). \quad (6)$$

For which, the total diffracted field located at the intersection of position vectors r_2^u and r_2^l in Fig. 3, corresponding to the vector summation of *E-fields* E_u and E_l may be expressed thus :

$$E_T(\mathbf{r},\omega) = \frac{E_u(v_u)e^{j[\omega t - \beta_0 r_u]}}{r_1^u r_2^u} + \frac{E_l(v_l)e^{j[\omega t - \beta_0 r_l]}}{r_1^l r_2^l}, \quad (7)$$

where β_0 is the free space propagation coefficient, and the vectors $r_u = r_u^1 + r_u^2$ and $r_l = r_l^1 + r_l^2$ represent the total path length from source to measurement position via the plate upper and lower edges. Normalising the summation of *E-field* components at all position vectors in (7) for identical upper / lower & left / right orthogonal edge pairings, enables the total energy propagating into the shadow region to be expressed as a fraction of total transmitted power through the aperture, i.e

$$H(\omega) = 2\sum_n^N \left|E_T(\mathbf{r}_n,\omega)\right|^2 \Big/ \left|E_o\right|^2 \cong pe^{[-r\omega]} + qe^{[-s\omega]}, \quad (8)$$

where $p = E_u(v_u)/r_1^u r_2^u$; $q = E_l(v_l)/r_1^l r_2^l$ etc. The parametric formulation on the RHS in (8), equivalent to the finite exponential series summation on the left, provides an approximate representation of the total diffracted field energy at all *N* sample positions within the modelled mesh space for both edge pair combinations. A close approximation to the rigorous solution may now be acquired via application of the inversion process [10] to yield coefficients p,q,r,s which provide an optimum fit to the interpolation surface defined in (8). In essence, this function, when convolved with the open aperture formulation in (2), defines that fraction of total incident *E-field* energy which propagates beyond the plate's geometric obstruction to ultimately be absorbed by the walls of the RAM enclosure.

B. Standing wave function

The characteristic standing wave pattern arising from the multiple reflections between aperture and plate [11] is deduced from the ray tracing schematic in Fig. 4 and may be expressed by the infinite time domain series:

$$r(t) = (1 - \rho_A) \otimes \left[\delta(t - t_0) - p_0 p_A \delta(t - 3t_0) + \ldots\right], \quad (9)$$

where ρ_o and ρ_A represent the equivalent reflection coefficients at plate and aperture impedance discontinuities respectively, whilst $t_0 = d/c_0$ is the propagation delay over distance *d* between aperture and plate. The resultant standing

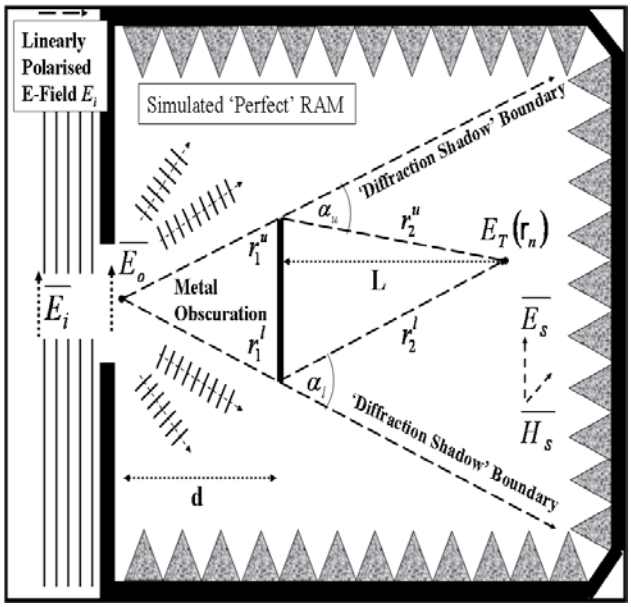

Fig. 3. Schematic showing Fresnel diffraction and plate obscuration geometry used to calculate the modified aperture transmission coefficient.

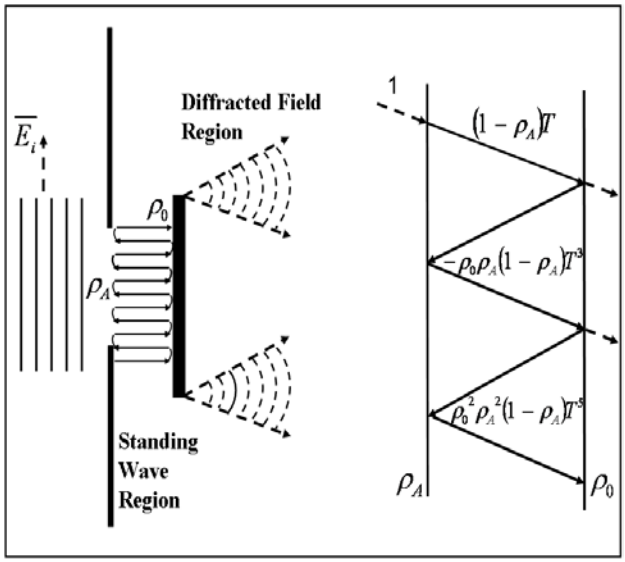

Fig. 4. Schematic of circular aperture and obstruction showing equivalent signal flow path model for multiple reflection and standing wave pattern evaluation.

wave function frequency dependence is derived from the FFT of (9) as:

$$R(\omega) = \left(1 - \rho_A(\omega)\right)\left[T - \rho_0(\omega)\rho_A(\omega)T^3 + ...\right], \quad (10)$$

where $T = \exp(-j\omega d/c_0)$ is the mesh space propagation coefficient. Note, in (10), $\rho_o(\omega) \approx -1$, is assumed to equal the reflection coefficient of the plate metallic conducting surface, whilst $\rho_A(\omega) \approx 1 - A_p(\omega)$, is derived via application of the unity property theorem [12] to the aperture transmission coefficient in (2). Finally, having evaluated the respective open aperture, standing wave pattern, and plate obscuration functions, the resultant transmission coefficient for the incident field $\boldsymbol{E_i}$ may be expressed as :

$$S_{OB}(\omega) = \eta_0 \left|A_p(\omega) H(\omega) R(\omega)\right|^2 \Big/ \left|E_i\right|^2 . \quad (11)$$

C. Obscuration simulation results

The obscuration coefficient of (11) was simulated using the CST microstripes TLM solver for a metal plate 50% larger than the aperture at displacements of 0.4 m, 0.6 m, and 0.8 m. The results are plotted and compared with their parametric, theoretical counterparts in Figs. 5, 6 and 7. Here, the attenuating effect of the plate and standing wave pattern attributable to the infinite series of reflections between impedance discontinuities at the aperture and plate itself are in evidence. Note, the decrease in the standing wave amplitude for an increase in plate displacement (d) from 0.4 to 0.8 m, and subsequent reduction in the diffraction boundary angle α, as less transmitted flux is caught in the plate shadow region and reflected. For large separations, as $d \to \infty$, T approaches zero and *R* tends to unity, the response asymptotically approaches that obtained in the absence of the plate. Both separations exhibit a good agreement between simulation and parametric theory.

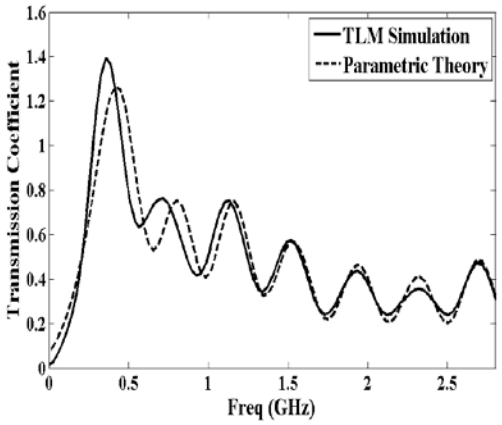

Fig. 5. Comparison between TLM simulation and parametric solution for a circular aperture model with obscuration plate at 400 mm separation.

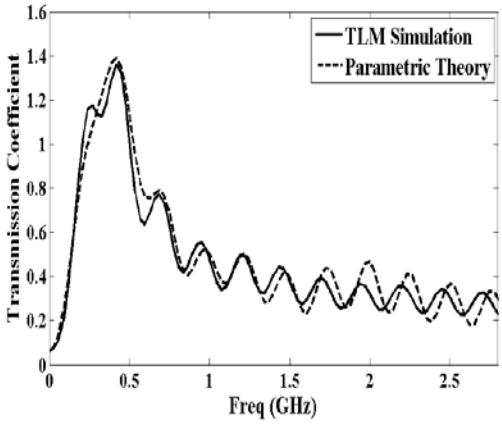

Fig. 6. Comparison between TLM simulation and parametric solution for a circular aperture model with obscuration plate at 600 mm separation.

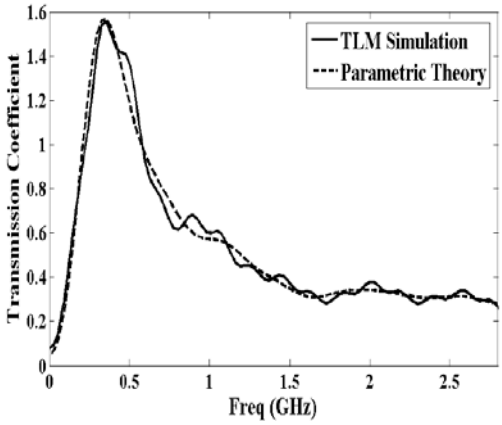

Fig. 7. Comparison between TLM simulation and parametric solution for a circular aperture model with obscuration plate at 800 mm separation.

V. CONCLUSIONS

This paper demonstrates how parametric expressions can greatly simplify the non-trivial computation of energy transfer through a circular aperture in a metal plate. The validity was confirmed via comparison with a standard TLM commercial solver model incorporating a virtual 'absorbing box' loss analysis algorithm. The method was further extended to accommodate modulation arising from the presence of obscurations, where both the characteristic geometrical shadowing and standing wave pattern associated with multiple reflections were recreated.

REFERENCES

[1] G. F. Koch and D. K. Kolbig, "Transmission Coefficient of Elliptical and Rectangular Apertures for Electromagnetic Waves," *IEEE Trans. Ant. and Prop.*, vol. AP-16, no. 1, Jan 1968.

[2] S. T. Imeci, F. Altunkilic, J. R. Mautz, and E. Arvas, "Transmission through an Arbitrarily Shaped Aperture in a Conducting Plane Separating Air and a Chiral Medium," *Applied Computational Electromagnetic Society (ACES) Journal*, vol. 25, no. 7, pp. 587 – 599, July 2010.

[3] S. R. Seshadri and T. T. Wu, "High Frequency Diffraction of Electromagnetic Wave by a Circular Aperture in an Infinite Plane Conducting Screen," *IRE Trans. Ant. Prop*, vol. AP-8, 1960.

[4] K. Hongo and Q. A. Naqvi, Diffraction of Electromagnetic Waves by Disk and Circular Hole in a Perfectly Conducting Plane, *Progress In Electromag. Research,* PIER 68, 113–150, 2007.

[5] CST STUDIO SUITE 2011, "Integrating Simulation Technology," *Microwave Journal*, vol. 53, no. 12, p. 92, December 2010.

[6] W. Andrejewski, "Die Beugung Elektromagnetischen Wellen an der Leitende Kreissheibe und an Der Kreisformigne ÌˆOffnung im Leitenden Ebenen Schirm," Z. Angew. Phys., vol. 5, 1950.

[7] D. A. Hill, M. T. Ma, A. R. Ondrejka, B. Riddle, M. L. Crawford, and R. T. Jonk, "Aperture Excitation of Electrically Large Lossy Cavities," *IEEE Trans. Electromagnetic Compatibility*, vol. 36, issue 3, pp. 169–179, 1994.

[8] I. Junqua and F. Issac, "Expérimentations sur RAFALE—Rapport d'essais," Technical Report ONERA RT 1/08212 DEMR, Sept. 2003.

[9] D. Parsons, *The Mobile Radio Propagation Channel*, pp. 35 to 45, Pentech Press, London 1992.

[10] M. Nakhkash, Y. Huang, and M. T. C. Fang, "Application of the Multi-Level Single Linkage Method to One-Dimensional EM Inverse Scattering," *IEEE Trans. Ant. and Prop*, p. 22, July 2003.

[11] F. Weinmann, "UTD Shooting-and-Bouncing Extension to a PO/PTD Ray Tracing Algorithm," *Applied Computational Electromagnetic Society (ACES) Journal*, vol. 24, no. 3, pp. 281 – 293, June 2009.

[12] S. Liao, *Microwave Devices and Circuits*, 2nd Edition, pp. 161-162, Prentice Hall, 1980.